Hybrid-Mode Analysis of Homogeneously and Inhomogeneously Doped Low-Loss Slow-Wave Coplanar Transmission Lines

Ke Wu, *Member, IEEE*, and Rüdiger Vahldieck, *Senior Member, IEEE*

Abstract—**A hybrid-mode analysis is presented to characterize the propagation properties of uniplanar slow-wave MIS coplanar transmission lines. The effect of homogeneous versus gradually inhomogeneous doping profile is investigated as well as the influence of the metal conductor losses and finite metallization thickness on the slow-wave factor and the overall losses. Numerical results indicate that thick-film MIS CPW's can support a slow-wave mode with moderate loss up to 40 GHz when the line dimensions are kept in the micrometer range. Furthermore, it is found that an inhomogeneous doping profile can reduce the overall losses and that the effect of metal conductor losses in heavily doped MIS structures is only marginal. On the other hand, in weakly doped or insulating GaAs material a lossy metal conductor leads to a higher propagation constant exhibiting a negative slope with increasing frequency. The numerical simulation is carried out by using the spectral-domain approach for lines with homogeneously doped semiconductor and the method of lines for the ones with inhomogeneously doped semiconductor, respectively. A self-consistent approach is used to represent lossy metal conductor planes.**

I. Introduction

UNILATERAL coplanar transmission lines are of growing interest for the design of monolithic microwave integrated circuits. In particular coplanar metal–insulator–semiconductor (MIS CPW) structures, which may support low-loss slow-wave propagation, have potential application in pulse delay circuits for phased arrays, in electronically controlled phase shifters and filters, and in reducing cross-coupling in high-speed digital integrated circuits, to name a few examples. Slow-wave propagation along coplanar MIS structures has been studied theoretically and experimentally by a number of authors [1]–[12].

The basic structure which supports a slow-wave mode is shown in Fig. 1 and consists of a multilayer coplanar transmission line on a thin semiconductor substrate which is homogeneously doped and is separated from the coplanar conductor plane by a low-loss or lossless insulating layer of silicon dioxide. The presence of a back metallization may or may not be considered. In any case, its influence on the propagation of a slow wave is negligible. The existence of a slow-wave mode in such a structure can be explained in the following way: The low-impedance semiconductor is virtually invisible to the magnetic field while the electric field is highly concentrated between the semiconductor and the center strip of the coplanar transmission line. This field distribution corresponds to a separate storage of electric and magnetic energy in space, which is the well-known condition for a low-loss slow-wave mode to propagate. The field concentration for this case is illustrated in Fig. 2, which shows the normalized power density distribution over the cross section of a thin-film MIS CPW deposited on a GaAs substrate. The power distribution is calculated using a spectral-domain approach [16]. As shown in Fig. 2(a), a large portion of the power density is located at and near the edge of the slot area at 0.1 GHz. While the power density at this location at interfaces 2 and 3 (see Fig. 1) is approximately the same, the power density in interface plane 1 is significantly smaller. The slow-wave mode disappears when the power density in interface 3 becomes significantly larger than that in interfaces 1 and 2. This is the case at 10 GHz and is illustrated in Fig. 2(b). At this frequency the power densities in interfaces 1 and 2 are almost identical while the power density in interface 3 is significantly higher. This means that the transmitted power is mainly concentrated in the semiconductor–insulator interface, which explains why the slow-wave mode is reduced from $\lambda_0/\lambda_g = 24.3$ ($\alpha = 0.23$ dB/mm) at 0.1 GHz to $\lambda_0/\lambda_g = 2.9$ ($\alpha = 5.53$ dB/mm) at 10 GHz. The latter value corresponds to a lossy dielectric mode.

For thin-film MIS transmission lines slow-wave propagation occurs mainly in the frequency range up to 1 GHz. Typical data are 0.2 dB/mm losses at 0.5 GHz and a slow-wave factor of 40 while losses increase at 4 GHz up to 10 dB/mm combined with a reduced slow-wave factor of 10 (for GaAs material). Extrapolating these results toward higher frequencies leads to the obvious conclusion

Manuscript received September 8, 1989; revised March 29, 1991. This work was supported in part by the National Science and Engineering Research Council of Canada (NSERC) under the Strategic Grant program.

The authors are with the Department of Electrical and Computer Engineering, University of Victoria, Victoria, B.C., Canada V8W 3P6.

IEEE Log Number 9101010.

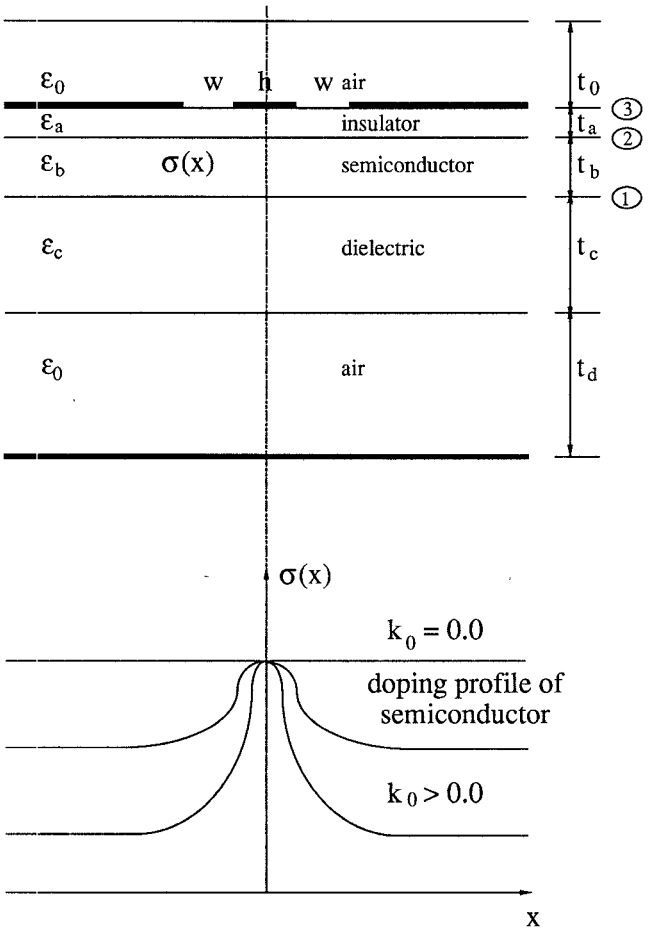

Fig. 1. Cross section of the thin- and thick-film MIS CPW structure with homogeneously and inhomogeneously doped semiconductor deposited on RT/Duroid or semi-insulating GaAs substrate ($t_0 = 10$ mm).

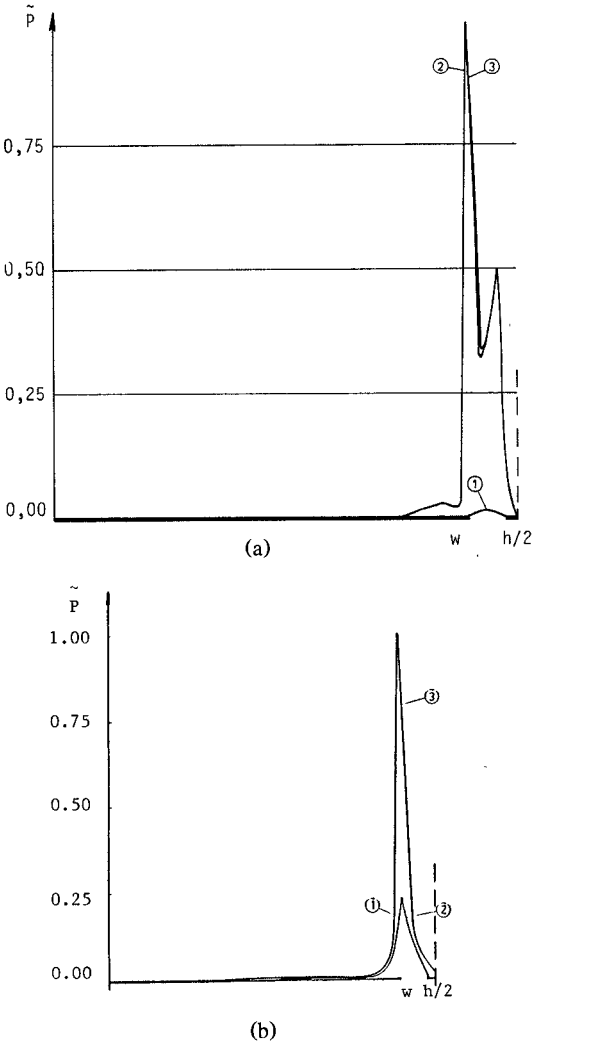

Fig. 2. Normalized power density at the three interfaces for a thin-film MIS CPW, as shown in Fig. 1, grown on GaAs substrate ($\epsilon_a = 8.5$, $\epsilon_b = \epsilon_c = 13.1$, $t_a = 0.3$ μm, $t_b = 0.7$ μm, $t_c = 360$ μm, $t_d = 0.0$, $w = 410$ μm, $h = 280$ μm, $\sigma = 12.8$ $(\Omega \cdot \text{mm})^{-1}$, ----: magnetic wall). (a) Real part at 0.1 GHz. (b) Real part at 10 GHz.

that those structures are not suitable for application at frequencies higher than 5 GHz.

To achieve low-loss slow-wave propagation also at higher frequencies, Kwon, Hietala, and Champlin [13], [14] proposed another version of the CPW structure, the so-called micrometer-size coplanar MIS transmission line, which is fabricated on a heavily doped thick N^+ silicon surface where a thin layer of SiO_2 is grown as insulator. In that paper some theoretical results based on a quasi-TEM approach together with experimental data up to 12 GHz were presented. Since the quasi-TEM approach becomes somewhat questionable at frequencies higher than 10 GHz, in the present paper a spectral-domain analysis was applied to determine the upper frequency limit of those structures. As a result of our analysis it was found that slow-wave mode propagation can theoretically be extended up to 40 GHz. Although fine line dimensions are necessary to realize this performance, which may lead to high fabrication cost, it is expected that with advanced process technology this structure may become of interest in the future. Therefore, in Section II of this paper design data will be given together with a more detailed discussion of the propagation characteristics in micrometer-size MIS CPW's.

An alternative approach for overcoming the problem of small line dimensions has been proposed by Wu [15]. In this solution the high doping region of the semiconductor in the MIS monolithic structure is limited to the region just below the center conductor instead of over the full cross section, as in [13] and [14]. For optimum results it was suggested to use a gradually inhomogeneous (Gaussian-like) doping profile which reaches a maximum level just below the center conductor (Fig. 1, in the case of $k_0 \neq 0$). Based on the theoretical analysis it was found that this solution is potentially suitable for reducing the losses of the slow-wave mode, which to a large extent is due to the electric field emerging from the strip area and its tangential component along the semiconductor interface. While the task in the homogeneously doped micro-size MIS CPW was to reduce this component by virtue of a reduced slot width, the inhomogeneous doping profile reduces only the effective lossy interface area by reducing the lateral expansion of the doped semiconductor. In

other words, the semiconductor–insulator interface under the strip changes very rapidly to an insulator–insulator interface with progressing distance from the strip area; hence the tangential component of the emerging electric field has less influence on the circuit losses. Therefore, the slot width need not be reduced to microsize dimensions.

Section III of this paper outlines the numerical procedure to analyze the propagation characteristics of the gradually inhomogeneously doped MIS CPW. Since the spectral-domain approach is not suitable for this task, the method of lines (MOL) has been adopted. It has been recognized very recently [22]–[26] that the effect of metal conductor loss may play a significant role for pulse propagation at lower frequencies; therefore this effect has been included in the analysis. This is particularly important when micrometer-size line dimensions are used which are of the order of the skin depth.

In Section IV numerical results based on the MOL are presented. Different doping profiles will be investigated to determine their effect on the slow-wave factor and semiconductor losses. Finally, we make use of results obtained by a self-consistent MOL to demonstrate the influence of the metal losses on the slow-wave factor and overall losses.

II. Design Aspects of Micrometer-Size, Homogeneously Doped MIS CPW

Homogeneously doped MIS CPW's have been studied extensively at frequencies below 10 GHz. Therefore, the first part of the following analysis, which is based on a spectral-domain approach assuming lossless metal conductor and no metallization thickness, focuses on a wider frequency range up to 40 GHz. Only structures which are deposited on SiO_2/Si thick-film heavily doped micro-dimensional MIS CPW are considered. This is for the following two reasons: First, it was found that this structure can support a slow-wave mode at moderate loss up to the millimeter-wave region; second, so far only little design information has been published for this version of the MIS CPW. The numerical procedure leading to the spectral-domain algorithm for this structure was published in [16] and is therefore omitted here for brevity.

The geometry of the central conductor, slots, and insulator layer in a micro-size MIS line are very small (several μm). While in a conventional thin-film MIS CPW the ratio between semiconductor layer and insulator thicknesses is typically in the range of 2:1 to 100:1, the micro-size MIS CPW is grown on a thick semiconductor and the insulator thickness ranges between 0.1 μm and 0.53 μm (ratio more than 1000:1). At the same time the strip width ranges from 5 to 10 μm, which is significantly smaller than in a conventional thin-film MIS CPW.

A. Frequency Characteristics

It was found in [13] that by optimizing the line dimensions and the doping level a moderate low-loss slow-wave mode can exist at frequencies higher than 5 GHz showing very little dispersion (quasi-TEM propagation). To predict the line parameters, a TEM model was developed in [14] which agrees well with measurements up to 10 GHz. For higher frequencies, however, the fluctuation of measured data around the predicted values increased significantly, which is an indication that this model is no longer valid. Therefore, we make use of the full-wave analysis [16] to determine the upper frequency limits of the micro-size MIS CPW. Fig. 3 illustrates the slow-wave propagation in a micro-size thick-film MIS CPW for different slot and strip widths. In comparison with the conventional thin-film MIS CPW, it is obvious from the figures that relatively low-loss slow-wave propagation can be expected up to 40 GHz when the slot and line widths are chosen very small ($w = 100$ μm, $h = 0.5$ μm, parts (a) and (b) of Fig. 3). For these dimensions the slow-wave factor remains above a moderate value of 15 with virtually no dispersion. The same observation can be made for the real part of the characteristic impedance, which shows only slight variations over the frequency but changes from $Z_r = 0.3$ Ω for a strip width of $h = 50$ μm to $Z_r = 18$ Ω for $h = 0.5$ μm. This effect is even more pronounced when the slot width decreases from $w = 100$ μm, in parts (a) and (b) of Fig. 3 to $w = 50$ μm, in parts (c) and (d). In the latter case losses of 5 dB/mm can be observed at 30 GHz together with a slow-wave factor of $\lambda_0/\lambda_g = 13$. The real part of the characteristic impedance varies now from $Z_r = 0.6$ Ω for $h = 50$ μm to $Z_r = 108$ Ω for $h = 0.5$ μm. At the same time the imaginary part of Z_0 can change from $Z_i = 0$ to 10 Ω. This behavior clearly indicates that in contrast to conventional thin-film structures the influence of the frequency on the field distribution in micro-size heavily doped MIS CPW's is significantly reduced. This is because the center conductor dimensions are considerably smaller than the guided wavelength in the frequency range up to 40 GHz. Therefore the electric field is mainly confined to the insulating layer below the center conductor (Fig. 1) and the distribution of the $\boldsymbol{E}$ field is similar to the quasi-static case. The magnetic field is to a good approximation the same as that of the CPW without a semiconductor. This also explains why the slow-wave effect appears virtually free of dispersion. Furthermore, the line loss, which is due to the skin effect ($\sqrt{2/\omega\mu\sigma}$) and the relaxation time ($2\pi\epsilon/\sigma$), is considerably reduced since the active surface in contact with the heavily doped semiconductor has the same size as the center conductor itself.

B. Influence of Line Parameters

As illustrated in [15], widening the strip leads to a higher slow-wave factor but at the same time the losses increase too. On the other hand, the complex characteristic impedance can be sensitively controlled by the slot width only as long as the center strip remains in the micro-size range, in general below 10 μm. To gain a better understanding of how the slow-wave characteristic

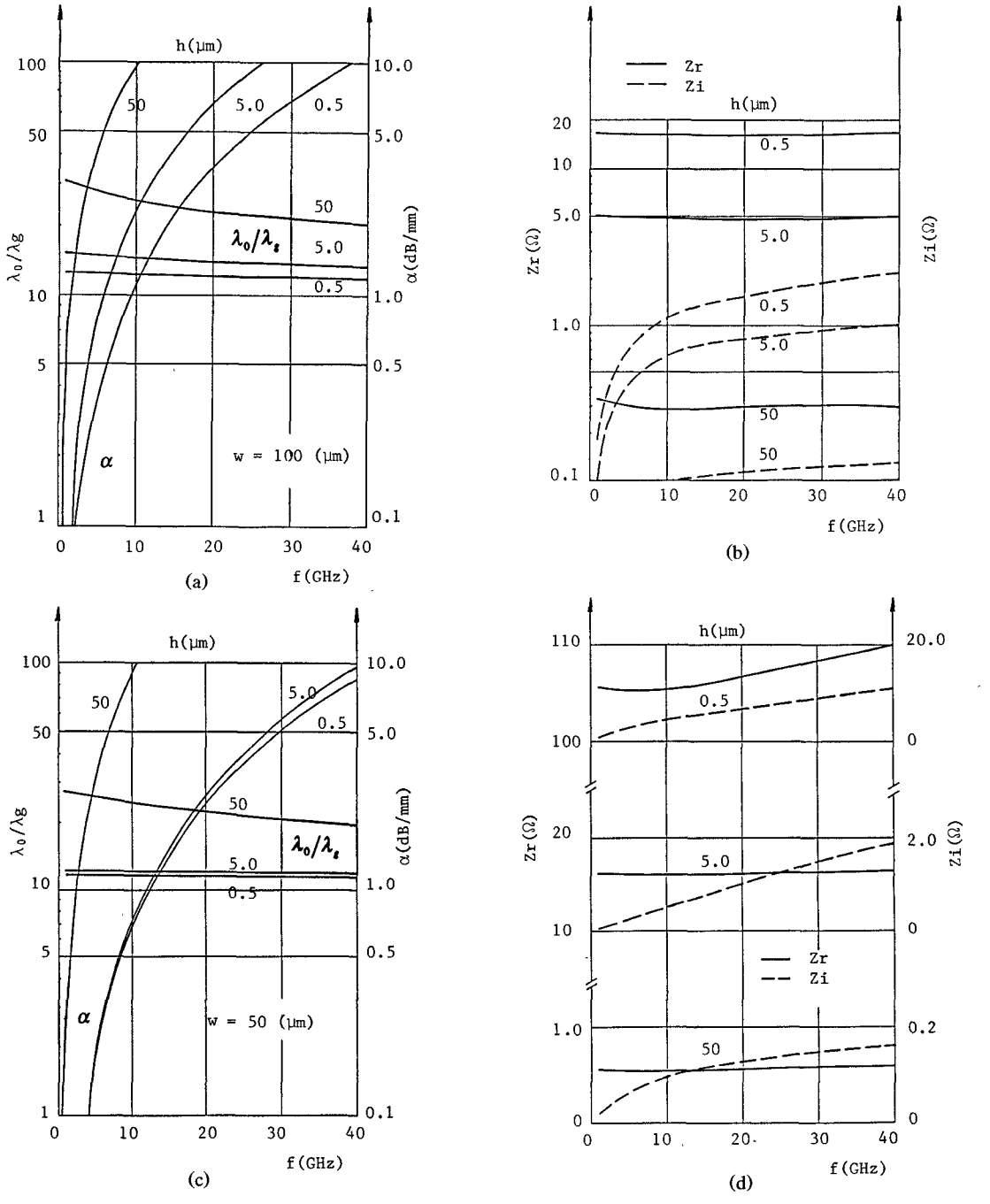

Fig. 3. Slow-wave factor, loss, and impedance characteristics as a function of frequency in a thick-film SiO_2/Si MIS CPW deposited on RT/Duroid substrate ($t_a = 0.1$ μm, $t_b = 150$ μm, $t_c = 660$ μm, $t_d = 0.0$, $\epsilon_c = 2.22$, $\sigma = 3.7037\ (\Omega \cdot \text{mm})^{-1}$).

depends on the geometry of a thick-film MIS CPW, the following investigation concentrates on the effect of the insulator thickness and the doping level of the semiconductor bulk because of their key influence on the slow-wave mode.

Fig. 4 illustrates the typical behavior of the propagation constant and complex impedance versus the insulator thickness, t_a. It can be seen that the losses decrease drastically when the insulator thickness increases but at the same time the slow-wave effect also tends to disappear (Fig. 4(a)). The losses decrease even more when the slot width is changed from $w = 100$ μm to $w = 10$ μm. This can be explained by remembering that a fraction of the electric field emerges from under the strip into the neighboring area with a component tangential to the semiconductor. It is this component which causes additional losses. When the slot width is reduced, an increasing portion of the emerging field is drawn into the slot area, thus reducing the part of the electric field which is tangential to the semiconductor surface; therefore also the losses are reduced. This variation in slot width exerts only a minor influence on the slow-wave factor but is significant with respect to the characteristic impedance, which, at the same time, changes by a factor of 10 (Fig.

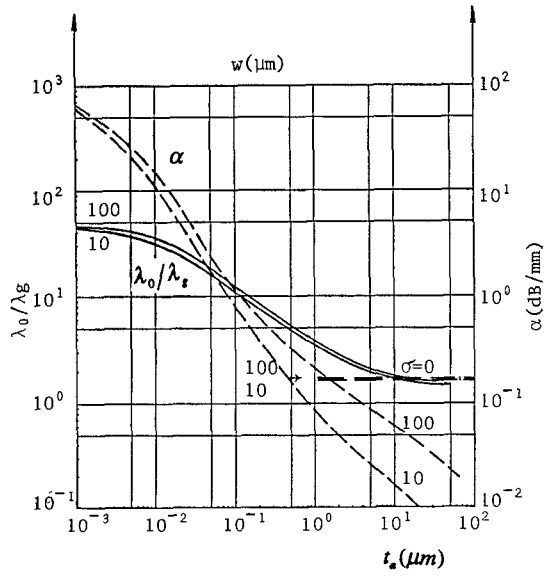

(a)

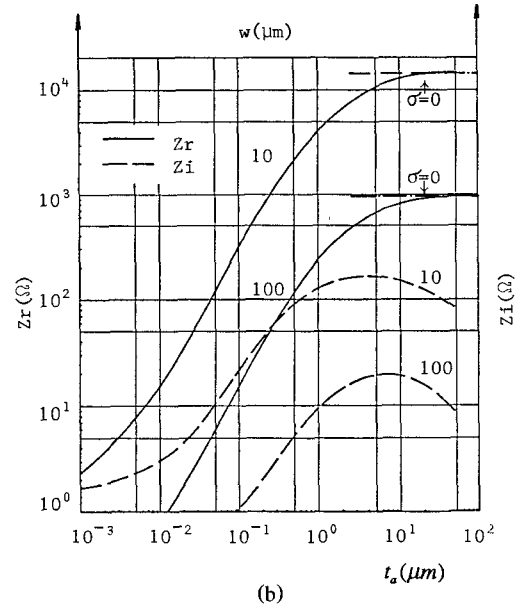

(b)

Fig. 4. Slow-wave factor, loss, and impedance characteristics versus insulator thickness t_a for $w = 10$ μm and 100 μm ($f = 10$ GHz, $h = 0.5$ μm).

4(b)). The real part of Z_0 shows saturation effects around $t_a = 10$ μm. At the same time the slow-wave mode tends to disappear when the center conductor width exceeds 10 μm. Based on these results, one can identify an optimum range for the insulator thickness of 0.03–0.5 μm to allow a slow-wave factor of 25–5 and losses between 5 and 0.2 dB/mm. Furthermore, it can be seen from Fig. 4 that for values of t_a larger than 10 μm the results converge to those for the lossless case ($\sigma = 0$), because the influence of the semiconductor on the field becomes negligible and consequently the phenomenon of field separation diminishes.

The loss and slow-wave factor also depend on the doping intensity of the semiconductor, as shown in Fig. 5.

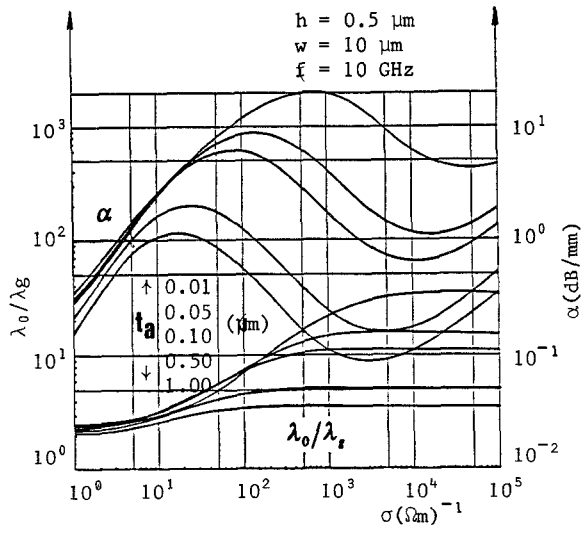

Fig. 5. Slow-wave factor and loss characteristics versus conductivity σ for different values of insulator thickness t_a.

It can be seen that a maximum slow-wave factor exists together with minimum losses in the heavy doping range of $\sigma = 10^3$–10^5 $(\Omega \cdot \mathrm{m})^{-1}$ for different t_a. It should be mentioned that this result is confirmed by experiments published in [14]. Fig. 6 illustrates the effect of the conductivity on the characteristic impedance. For conductivity values smaller than $\sigma = 10^2$ $(\Omega \cdot \mathrm{m})^{-1}$ the real part of Z_0 remains relatively high ($Z_r = 500$ Ω at $t_a = 0.01$ μm) and less sensitive to the insulator thickness while the imaginary part varies strongly with σ. Within the optimum range of insulator thicknesses there is a certain amount of flexibility in choosing the structural dimensions of the MIS CPW. For instance, at $\sigma = 10^4$ $(\Omega \cdot \mathrm{m})^{-1}$ the loss factor ranges from 0.1 dB/mm to approximately 10 dB/mm for $t_a = 1.0$ μm and $t_a = 0.01$ μm, respectively. It is interesting to note that the low-loss slow-wave propagation usually occurs in case of $Z_l \approx 0$, which can be explained by the fact that the reactive power is reduced to a minimum value and thus decreases the relaxation time, RC.

III. Method of Lines Analysis of Inhomogenously Doped MIS CPW

An obvious disadvantage of the homogeneously doped MIS CPW is that the common impedance range of 50 Ω requires ultrafine line dimensions, which could impose manufacturing problems. As will be shown later, inhomogeneous doping of the semiconductor may solve this problem to a certain extent. The spectral-domain approach as used in the homogeneously doped thick-film structure is not suitable for analyzing this type of structure. Therefore, we use the method of lines combined with a nonequidistant discretization (Fig. 7). Compared with the equidistant discretization, this approach reduces considerably the memory space and CPU time requirements. This is a particularly important aspect in the numerical analysis of microdimensional MIS transmission lines, because a

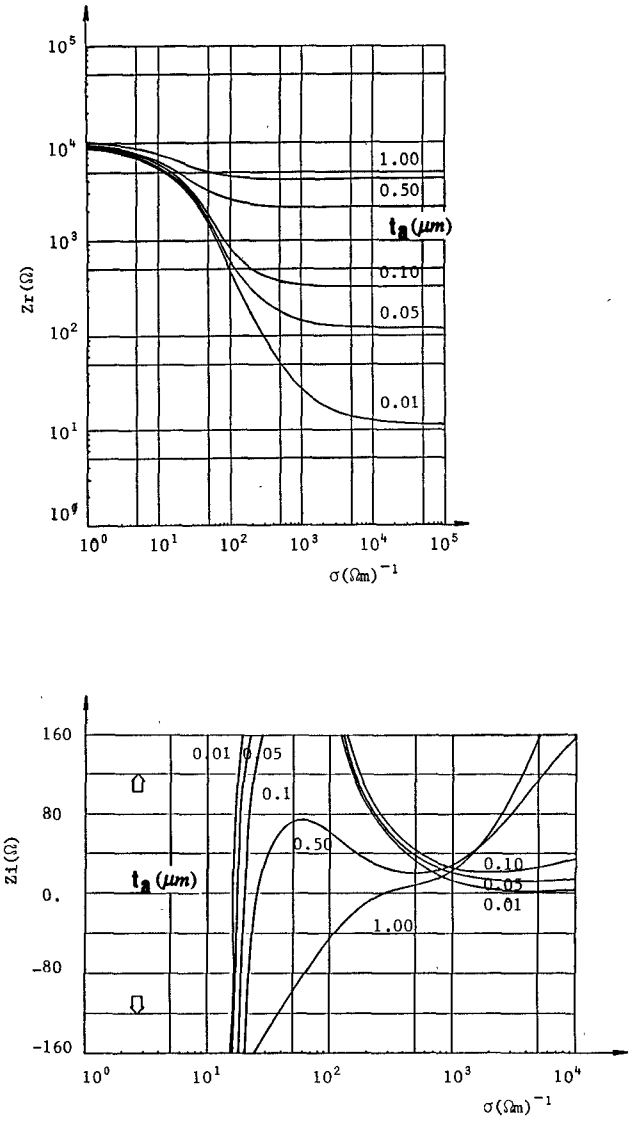

Fig. 6. Characteristic impedance versus conductivity σ for different values of insulator thickness t_a.

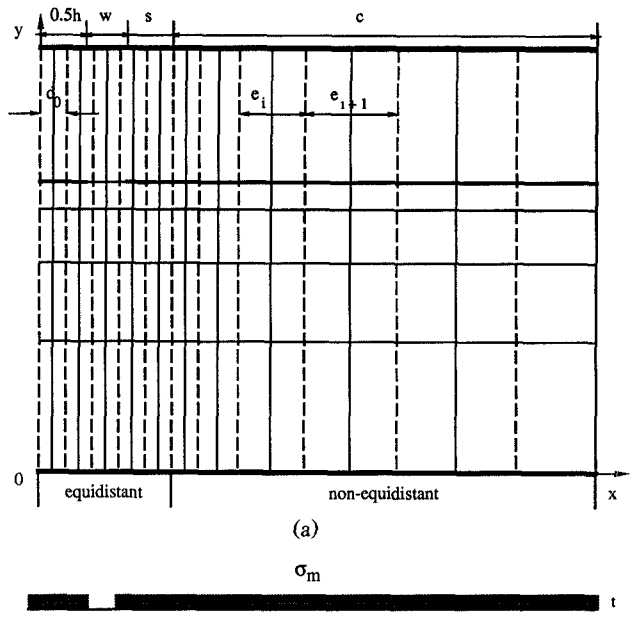

Fig. 7. Cross section of the coplanar MIS CPW with equidistant and nonequidistant discretization scheme used in the method of line analysis. (a) Structure with zero metallization thickness. (b) Finite metallization thickness treated as conductive dielectric layer in the self-consistent approach. ($s + c \geq 100\times$ and $10\times(w + 0.5h)$ for all following structures.)

high line resolution is required in the strip/slot region. If we assume symmetry of the structure and concentrate our analysis on the fundamental mode only, the Neumann–Dirichlet condition can be imposed, which means magnetic and electric walls are assumed as lateral boundaries. This step simplifies the formulation significantly and leads to a square matrix analysis. Since a detailed discussion of this approach has been presented in [17]–[20], only those steps in the formulation which are related to the inhomogeneous doping distribution $\sigma(x)$ will be given.

A. Analytical Formulation

The MIS CPW cross section is divided into two subregions, the equidistant discretization region with an interval size of d_0 between lines and the nonequidistant discretization area for which the line distance is calculated in the following way:

$$e_{i+1} = e_i + q \cdot d_0 \qquad (q \text{ a positive scaling coefficient}). \tag{1}$$

Along each of these lines the electric field components E and H are derived from two independent TE and TM scalar potential functions, ψ^e and ψ^h, which must satisfy both the scalar Helmholtz and the Sturm-Liouville equation, respectively [19], [20]:

$$\frac{\partial^2\psi^h}{\partial y^2} + \frac{\partial^2\psi^h}{\partial x^2} + \left(\epsilon_r(x)k_0^2 - \beta^2\right)\psi^h = 0$$

$$\frac{\partial^2\psi^e}{\partial y^2} + \epsilon_r(x)\frac{\partial}{\partial x}\left(\frac{1}{\epsilon_r(x)}\frac{\partial\psi^e}{\partial x}\right) + \left(\epsilon_r(x)k_0^2 - \beta^2\right)\psi^e = 0 \tag{2}$$

with $k_0^2 = \omega^2\mu_0\epsilon_0$ and β the unknown propagation constant. Note that dielectric losses caused by the semiconductor doping are included in these equations as the imaginary part of the dielectric permittivity. The basic idea of the MOL is to decouple the Helmholtz and Sturm–Liouville partial differential equations in (2) in the discrete space domain by means of an appropriate transformation such that both equations can be written in a set of analytically solvable ordinary differential equations of

the following form:

$$\frac{d^2\vec{V}^{e,h}}{dy^2} - \bar{k}_{e,h}^2\vec{V}^{e,h} = 0 \tag{3}$$

with $\bar{k}_{e,h}^2$ a diagonal matrix. The following discussion addresses mainly the diagonalization process for the matrix $\bar{k}_{e,h}^2$ in the semiconductor layer, because for the homogeneous layer it has already been explained in some detail [18]. To begin with, the first step in the procedure is to discretize the potential functions, then normalize the ones that are related to the nonequidistant discretization area, and finally transform them so that they can be written in the following vector form:

$$\vec{\psi}^{e,h} = \gamma^{e,h}T^{e,h}p^{e,h}\vec{V}^{e,h} \tag{4}$$

with

$$\gamma^{e,h} = \operatorname{diag}\left(\sqrt{d_0/e_i, h_i}\right). \tag{5}$$

$T^{e,h}$ denotes the orthogonal transformation matrix [18] and $p^{e,h}$ is an additional complex eigenmatrix to take into account the inhomogeneously doped semiconductor. For the area of equidistant discretization, $e_i = h_i = d_0$.

After the normalization and transformation procedure, the x-dependent term in (2) can be written in matrix form:

$$\gamma^{e^{-1}}\left\{\epsilon_r(x)\frac{\partial}{\partial x}\left(\frac{1}{\epsilon_r(x)}\frac{\partial\psi^e}{\partial x}\right) + \epsilon_r(x)k_0^2\psi^e\right\} \Rightarrow \left(-\frac{\bar{\epsilon}^e D_x^t \bar{\epsilon}^{h^{-1}} D_x}{d_0^2} + \bar{\epsilon}^e k_0^2\right)T^e p^e \vec{V}^e$$

$$\gamma^{h^{-1}}\left\{\frac{\partial^2\psi^h}{\partial x^2} + \epsilon_r(x)k_0^2\psi^h\right\} \Rightarrow \left(-\frac{D_x D_x^t}{d_0^2} + \bar{\epsilon}^h k_0^2\right)T^h p^h \vec{V}^h. \tag{6}$$

The terms D_x denote the normalized finite difference matrices resulting from the discretization procedure. The diagonal matrices $\bar{\epsilon}^h$ and $\bar{\epsilon}^e$ represent the discretized complex dielectric permittivity. The matrix product on the right-hand side in (6) is still tridiagonal. Diagonalizing the matrix for the homogeneous layer is achieved simply by applying the orthogonal matrix $T^{e,h}$. For the inhomogeneous layer, however, an additional transformation is required since the matrix product on the right-hand side of (6) is still not diagonal. This can be achieved by applying the complex eigenmatrix $p^{e,h}$:

$$T^{e^t}\left\{\left(-\frac{\bar{\epsilon}^e D_x^t \bar{\epsilon}^{h^{-1}} D_x}{d_0^2} + \bar{\epsilon}^e k_0^2\right)T^e p^e \vec{V}^e\right\} \Rightarrow \left(-\frac{\tilde{\epsilon}^e \delta^t \tilde{\epsilon}^{h^{-1}}\delta}{d_0^2} + \tilde{\epsilon}^e k_0^2\right)p^e \vec{V}^e$$

$$T^{h^t}\left\{\left(-\frac{D_x D_x^t}{d_0^2} + \bar{\epsilon}^h k_0^2\right)T^h p^h \vec{V}^h\right\} \Rightarrow \left(-\frac{\delta\delta^t}{d_0^2} + \tilde{\epsilon}^h k_0^2\right)p^h \vec{V}^h. \tag{7}$$

The new terms in (7) are

$$\delta = T^{h^t} D_x T^e$$

$$\tilde{\epsilon}^e = T^{e^t}\bar{\epsilon}^e T^e$$

$$\tilde{\epsilon}^h = T^{h^t}\bar{\epsilon}^h T^h. \tag{8}$$

The eigenmatrix $p^{e,h}$ can be determined by using the QR algorithm in such a way that the matrix $\bar{k}_{e,h}^2$ becomes diagonal:

$$\bar{k}_e^2 = p^{e^{-1}}\left(\frac{\tilde{\epsilon}^e \delta^t \tilde{\epsilon}^{h^{-1}}\delta}{d_0^2} - \tilde{\epsilon}^e k_0^2\right)p^e + \beta^2 \bar{I}$$

$$\bar{k}_h^2 = p^{h^{-1}}\left(\frac{\delta\delta^t}{d_0^2} - \tilde{\epsilon}^h k_0^2\right)p^h + \beta^2 \bar{I}. \tag{9}$$

Equations (4) to (9) have outlined the diagonalization procedure for matrix $\bar{k}_{e,h}^2$ in (3). The solution to (3) corresponds now to a set of simple transmission line equations in the transformed domain in the y direction. This provides a simple means of directly linking the transformed electric/magnetic potentials at the two boundaries within a subregion. After matching the transformed tangential field components at each interface, a matrix relationship can be established between two subregions. Finally, by successively multiplying those matrices with the related transmission line matrices, two matrix equations can be established, one relating the fields at the top housing wall to the strip/slot interface plane and the other relating the bottom housing wall to the strip/slot interface plane. After some mathematical manipulations, both matrix equations are reduced to a single algebraic coupled Green's function matrix in the transform domain (in the slot/strip interface):

$$\begin{bmatrix}\vec{e}_x \\ \vec{e}_z\end{bmatrix}\begin{bmatrix}y_{xx} & y_{xz} \\ y_{zx} & y_{zz}\end{bmatrix} = \begin{bmatrix}\vec{j}_x \\ \vec{j}_z\end{bmatrix}. \tag{10}$$

Transforming (10) back into the original space domain and setting the tangential modal current in the slot area to zero leads to the characteristic matrix equation system for which the nontrivial solutions of its determinant must be sought. The potential lines intersecting the slot area are limited to a relatively small number necessary to obtain convergence. This number directly determines the size of the characteristic matrix equation system.

For the structure to be studied in this paper we have chosen a doping distribution as follows:

$$\sigma(x) = \begin{cases} \sigma_0\left(ch\dfrac{x}{h}\right)^{-k_0} & \text{for } (|x| \leq 0.5h + w + s) \\ \sigma_0\left(ch\dfrac{0.5h + w + s}{h}\right)^{-k_0} & \text{for } (|x| > 0.5h + w + s) \end{cases} \tag{11}$$

in which a positive value of k_0 determines the inhomogeneous doping profile and σ_0 the maximum doping level. It should be noted that this function does not necessarily

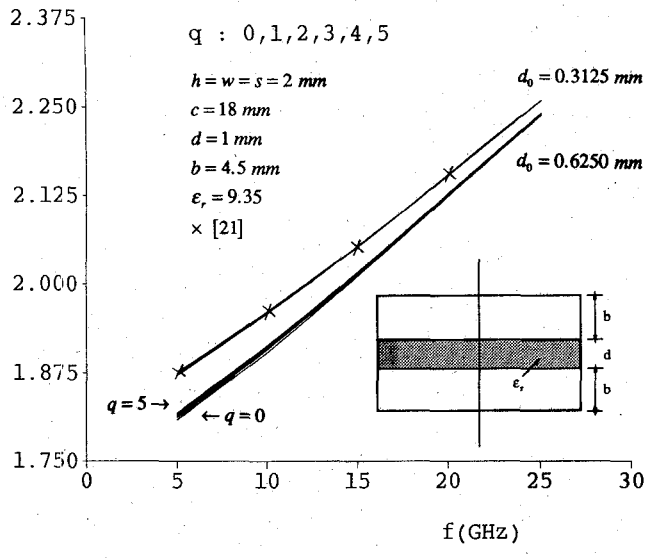

Fig. 8. Convergence behavior of the frequency-dependent propagation constant λ_0/λ_g with different gradual scaling factors.

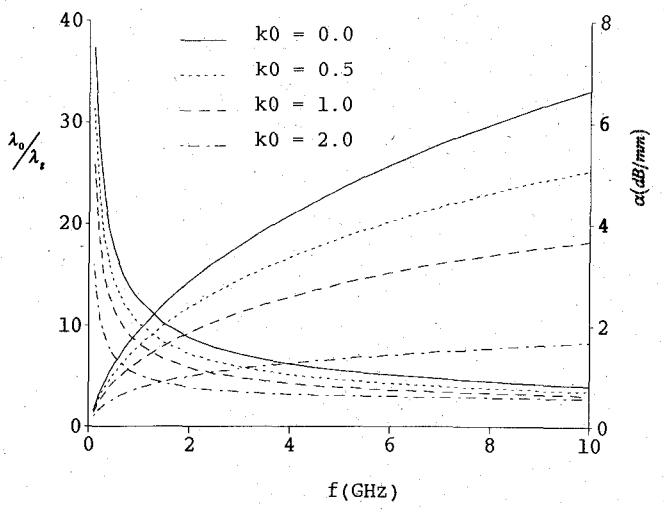

Fig. 9. Frequency-dependent slow-wave and loss factors for inhomogeneously doped thin-film MIS structures and different doping distributions ($\sigma_0 = 12.8\,(\Omega\cdot\text{mm})^{-1}$). Dimensions and parameters for all thin-film structures as in Fig. 2, except $t_d = 5.0$ mm.

describe the optimum doping distribution for all kinds of slow-wave structures. The best function for optimum low-loss slow-wave propagation depends on the type of MIS transmission line and also on the ratio of structural dimensions.

To include a lossy conductor of finite metallization thickness in the numerical analysis, we make use of a so-called self-consistent approach to the MOL. The analytical formulation is similar to the one presented above except that $\text{LSE}_x/\text{LSM}_x$ potential functions are used instead of the TE/TM approach. The term *self-consistent* means that the lossy conductor with finite metallization thickness is treated as a lossy dielectric layer with high conductivity (Fig. 7(b)). Details of this approach are beyond the scope of this paper. The interested reader is referred to [22] and [24]. Only results from this approach will be discussed in the following sections.

B. Convergence Behavior

Fig. 8 shows a convergence analysis of the normalized propagation constant for different discretization schemes in a conventional CPW. For narrowly spaced equidistant lines in the strip–slot region ($d_0 = 0.3125$ mm) and different scaling factors q, ranging from $q = 0$ (equidistant discretization outside the strip–slot region) to $q = 5$ (very coarse nonequidistant discretization, see also (1)), the error is virtually negligible. The error increases up to 1% if the equidistant line spacing in the strip–slot region is increased by a factor of 2. Changing the parameter for nonequidistant discretization outside the strip–slot area has only a minor effect on the overall convergence. This is because most of the electromagnetic field is concentrated in the strip–slot area. Consequently, all the following investigations have been performed by using eight $\psi^{e,h}$ lines in the strip–slot area and up to five $\psi^{e,h}$ lines outside.

IV. Results for Inhomogeneously Doped MIS CPW

It is known from the previous analysis that thin- and thick-film MIS CPW's have their own distinctive behavior in terms of losses and slow-wave propagation. In general, the thin-film MIS CPW supports a low-loss slow-wave mode only at lower frequencies (usually below 1 GHz), while in a thick-film structure a slow-wave mode can be maintained up to the lower portion of the millimeter-wave region. Therefore, both structures are analyzed separately.

A. Thin-Film MIS CPW

Fig. 9 shows the slow-wave factor and the line losses versus frequency in a thin-film MIS CPW with homogeneous ($k_0 = 0$) and gradually inhomogeneous doping profiles ($k_0 = 0.5$–2). As expected, the slow-wave factor reduces significantly with increasing frequency and becomes a dielectric mode beyond 2 GHz. This effect becomes more pronounced by narrowing the shape of the doping profile. At the same time a narrower doping profile improves the loss factor significantly. Both results can be explained by the fact that a sharp doping lobe cannot grasp the electric field sufficiently because of a considerably reduced effective active surface area below the center conductor. In other words, the electric field is dispersed into the cross section in a way similar to that of the magnetic field; hence the condition for a slow-wave mode to propagate, namely the separate storage of magnetic and electric energy in space, is no longer satisfied. Fig. 10 shows relative values of the line quality factor, Q, which is defined by $Q = (\alpha\cdot\lambda_g)^{-1}$, for different doping profiles. At frequencies where the slow-wave mode is most sensitive to the doping profile, the Q factor shows no significant improvement. At frequencies higher than 2 GHz, the slow-wave mode approaches the dielectric mode

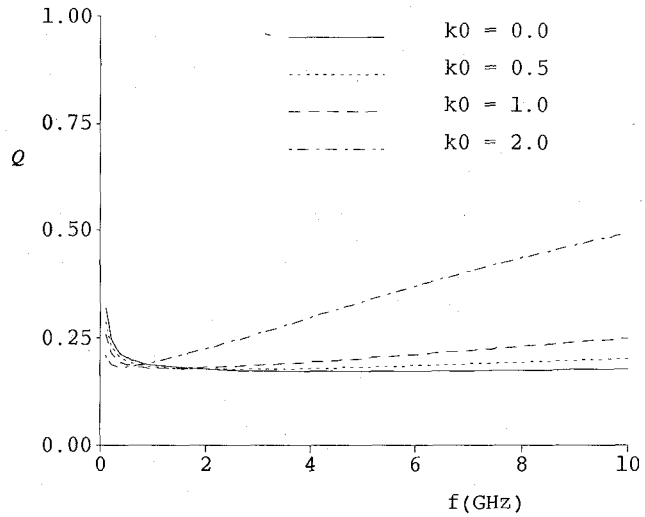

Fig. 10. Relative line quality for thin-film MIS structures.

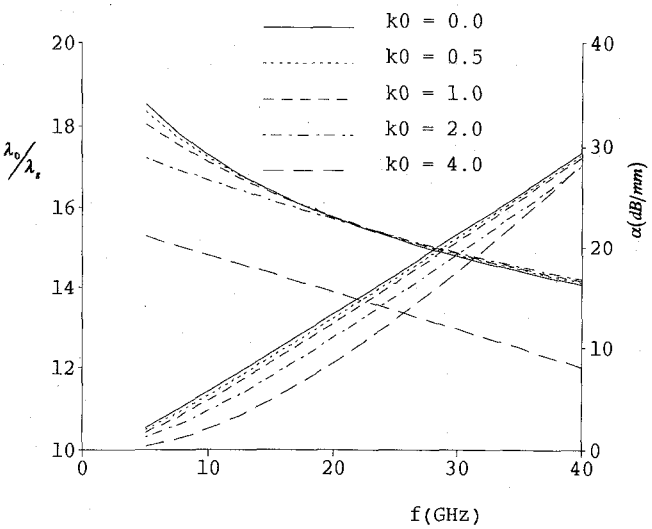

Fig. 11. Slow-wave and loss factors of the inhomogeneously doped thick-film MIS structures versus frequency ($\sigma_0 = 10.0\ (\Omega \cdot \text{mm})^{-1}$). Dimensions and parameters for all thick-film structures as in Fig. 3, except $h = w = 50\ \mu\text{m}$, $t_d = 5.0$ mm, $t_a = 0.2\ \mu\text{m}$.

and the losses decrease considerably if the doping profile is made very narrow. This leads to an increase of the Q factor with progressing frequency.

B. Thick-Film MIS CPW

Fig. 11 illustrates the behavior of the slow-wave mode in a thick-film MIS CPW over a range of 40 GHz. Two observations can be made: First, the slow-wave mode is less dispersive than in a thin-film MIS CPW and can be maintained beyond 30 GHz; second, the doping profile has less influence on the slow-wave mode. Only a very narrow doping profile ($k_0 = 4$) reduces the slow-wave mode significantly. The reason for this behavior has been explained previously in conjunction with the thin-film MIS CPW. The line losses, however, are more sensitive to the doping profile. Loss reduction of 5 dB/mm can be achieved if the doping profile index, k_0, is changed from

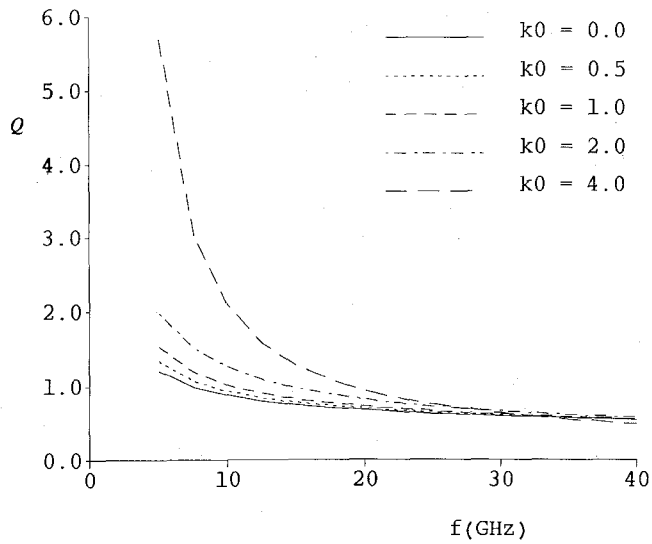

Fig. 12. Relative line quality for thick-film MIS structures.

$k_0 = 0$ (homogeneous doping distribution) to $k_0 = 4$ (very narrow doping profile). Comparing this figure with Fig. 3(c) shows clearly that by using a relatively wide center conductor (50 μm) the inhomogeneous doping profile allows a low-loss slow-wave mode ($\alpha < 10$ dB/mm) up to 20 GHz. For the structure in Fig. 3(c), this was possible only by reducing the center strip width to 10 μm or less.

Fig. 12 illustrates the line quality factor versus the frequency. It is interesting to note that for frequencies higher than 30 GHz the influence of the doping profile on the Q factor is virtually negligible. This may be explained by the fact that at higher frequencies the electric field is increasingly concentrated below the center conductor so that the doping profile outside this region has less influence on the field.

V. Effect of Metal Conductor and Semiconductor Losses

It is known that with decreasing line width, the metal conductor losses increase. Since the analysis of the microdimensional MIS CPW presented in Section II did not include this effect, the following section investigates the influence of both the metal conductor and the semiconductor losses on the overall loss behavior and the slow-wave factor in a thick-film MIS CPW.

In the past, the perturbation method and the surface impedance approach were widely used in the literature to determine metal conductor losses. Their accuracy, however, become questionable in view of the fact that the metallization thickness in the MIS CPW is not always large in comparison with the skin depth. The following results are therefore based on a self-consistent description of metallic losses [24] together with a full-wave analysis, in this case the MOL. This approach treats the conductor as a lossy dielectric layer of high conductivity and hence is not based on any approximation.

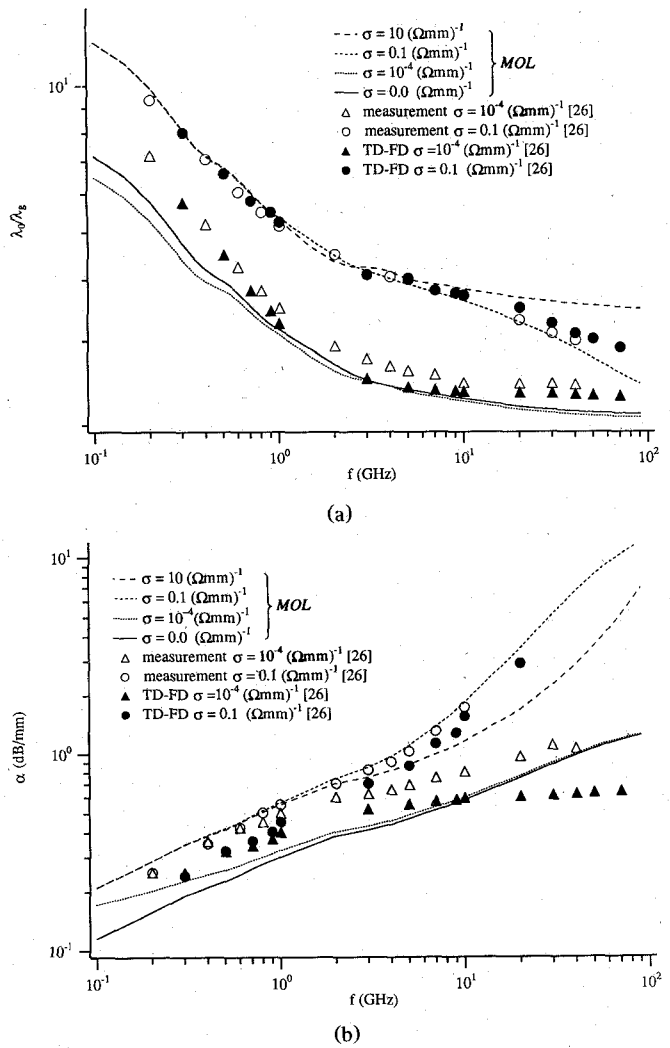

Fig. 13. A comparison of measured and calculated results of bulk, weakly, medium, and strongly doped SiO_2/Si MIS CPW including lossy conductor (low-density Al $\sigma_m = 2.7\times10^4$ $(\Omega\cdot\text{mm})^{-1}$) with finite thickness $t = 0.8$ μm ($h = 10$ μm, $w = 5$ μm, $t_a = 1.0$ μm, $t_b = 480$ μm, $t_c = 0.0$, $t_d = 5.0$ mm).

A. Loss Effect of Doped Semiconductors

To begin with, we first examine the effect of the semiconductor loss on the slow-wave factor and the overall loss for different levels of doping. The metal conductor is included in the analysis and during this part of the investigation consists of low-density Al with $\sigma = 2.7\times10^4$ $(\Omega\cdot\text{mm})^{-1}$. Fig. 13 shows the frequency-dependent slow-wave characteristic for different (homogeneous) doping levels. A comparison is made between the MOL results and results obtained from a FDTD analysis [26], which was published recently together with measurements. The MOL results are in good agreement with the measurements and generally also with the FDTD results. It is furthermore evident from Fig. 13(b) that the loss characteristic measured in [26] is in even better agreement with results obtained from our MOL analysis than with the FDTD prediction published in the same paper.

It should be noted that the results published in [26] only deal with weakly and very weakly doped thick-film MIS CPW structures ($\sigma = 10^{-4} \sim 0.1$ $(\Omega\cdot\text{mm})^{-1}$). Unfortunately, the authors have made no comparison with the heavily doped thick-film MIS CPW in [13] and [14]; nor have they mentioned this work at all. Therefore, Fig. 13 illustrates also the transmission properties for heavily doped ($\sigma = 10$ $(\Omega\cdot\text{mm})^{-1}$) as well as insulating ($\sigma = 0.0$ $(\Omega\cdot\text{mm})^{-1}$) semiconductor bulk. It is interesting to see that from 10 to 100 GHz the heavily doped MIS CPW displays clearly better performance (higher slow-wave factor together with lower losses and relatively little dispersion) than the weakly doped ($\sigma \leqslant 0.1$ $(\Omega\cdot\text{mm})^{-1}$) structure. In particular the loss factor of the heavily doped line ($\sigma = 10$ $(\Omega\cdot\text{mm})^{-1}$) is reduced by nearly 3 dB/mm at 30 GHz over the weakly doped ($\sigma = 0.1$ $(\Omega\cdot\text{mm})^{-1}$) case. On the other hand, both the heavily doped and the weakly doped semiconductors show very similar characteristics at frequencies below 1 GHz.

B. Loss Effect of Nonideal Conductors

To answer the question whether and to what extent the slow-wave factor is affected by the metal conductor loss, we consider the two cases of weakly doped ($\sigma = 10^{-4}$ $(\Omega\cdot\text{mm})^{-1}$) and insulating bulk semiconductors ($\sigma = 0.0$ $(\Omega\cdot\text{mm})^{-1}$), also illustrated in Fig. 13. First of all it should be noted that in both cases the propagation constant is not associated with a slow-wave mode. For the insulating semiconductor bulk and a lossy metal conductor it is surprising to see that, in contrast to classic results, a negative slope (Fig. 13(a)) of the propagation constant occurs at lower frequencies. This phenomenon is also backed by two recent experiments [25], [26]. A possible explanation for this behavior may be that at low frequencies the skin depth, δ, is relatively large, allowing the current to penetrate deeper into the conductor (usually $t \sim 2\delta$). In this situation the metal acts more like a semiconductor, influencing the propagation constant as a doped semiconductor layer would influence the slow-wave factor over the frequency. A slightly different but perhaps more plausible explanation, leading to the same results, may be that the current penetration deeper into the metal surface increases the inductance per unit length of line. This would slow down the phase velocity and increase the propagation constant. With increasing frequency, however, this mechanism would lose its effect (as shown in Fig. 13) since the skin depth decreases. Comparing the effect of the weakly doped and the insulating semiconductor layer, Fig. 13 seems to suggest that a lossy metal conductor can yield a higher propagation constant than a very weakly doped MIS CPW. This observation could lead to the assumption that a lossy metal conductor could increase the slow-wave factor in a heavily doped semiconductor line.

To investigate the extent to which this assumption is true, Figs. 14 and 15 compare the slow-wave factor and overall losses in thin- and thick-film MIS CPW's on heavily doped semiconductor material, considering a lossy metal conductor of finite thickness. It is interesting to

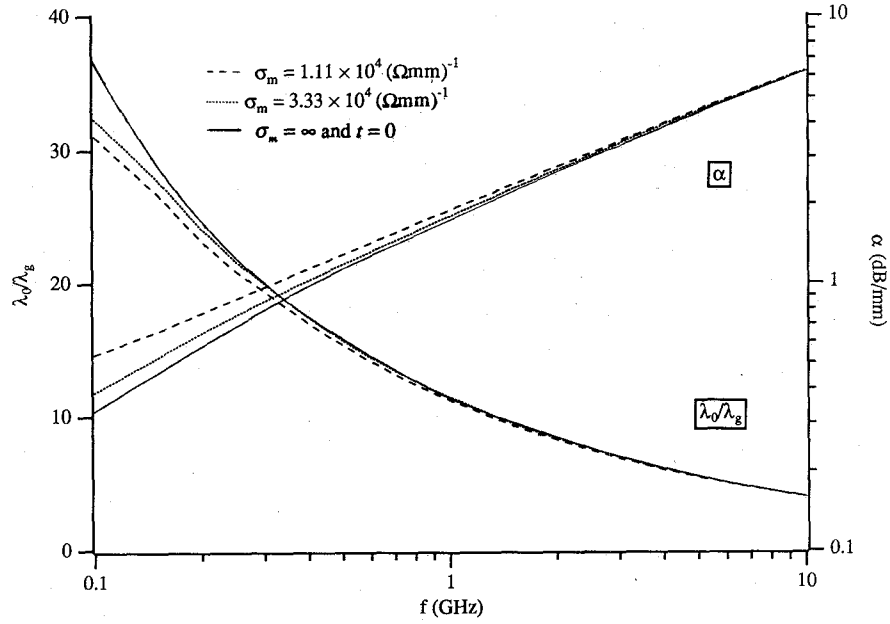

Fig. 14. Frequency-dependent slow-wave factor and loss characteristics of thin-film MIS CPW lines for different conductors ($t = 1.5\ \mu$m). Dimensions and parameters as in Fig. 9.

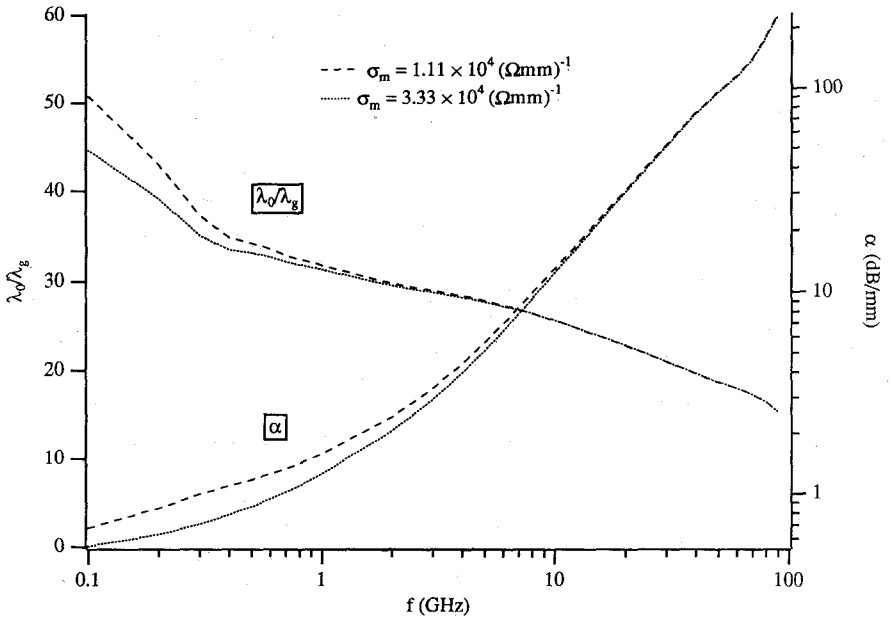

Fig. 15. Frequency-dependent slow-wave factor and loss characteristic of thick-film MIS CPW lines for different conductors ($t = 1.5\ \mu$m). Dimensions and parameters as in Fig. 3 ($w = h = 50\ \mu$m).

note that in both structures the transmission characteristics are indeed affected by the amount of metal conductivity but in opposite directions. In the thin-film structure a smaller metal conductivity lowers the slow-wave factor up to approximately 1 GHz (at higher frequencies the effect diminishes) while exactly the opposite effect is observed for the thick-film transmission line up to 5 GHz. The overall losses are increased in both cases. Fig. 14 shows also the influence of a lossless metal conductor of zero thickness. Compared with the finite-thickness metal conductor of good quality (usually gold or high-density Al, $\sigma = 3.33 \times 10^4\ (\Omega \cdot \text{mm})^{-1}$), the difference is less than 5% at lower frequencies. This result suggests that the data presented in Section II, which assumes a lossless and zero thickness metal conductor, are suitable for design purposes.

VI. Conclusion

Based on the spectral-domain approach we have presented a selection of design data for microsize homogeneously doped thick-film MIS coplanar transmission lines. It has been shown that this type of structure is superior to traditional thin-film MIS transmission lines for the follow-

ing reasons: 1) the slow-wave mode operation can be extended up to 40 GHz with moderate overall loss; 2) the slow-wave mode exhibits very little dispersion over an extremely wide frequency band.

To overcome the microsize dimensions and to reduce the losses even further, gradually inhomogeneous doping of the thick-film MIS CPW has been introduced. The analysis procedure for this type of transmission line is based on the method of lines using a nonequidistant discretization. The analysis includes the finite metallization thickness and losses of the metal conductor by using a self-consistent approach. First, it was shown that, depending on the doping profile, the microsize dimensions of the thick-film MIS CPW can be relaxed by a factor of 5. Second, the loss mechanism introduced by the semiconductor and the lossy metal conductor has been investigated separately. It was found that in a thin-film structure a lossy metal conductor reduces the slow-wave effect while the opposite is true in a thick-film transmission line. For the special case of an insulating semiconductor and considering only the losses introduced by the metal conductor, it was most surprising to see that the propagation constant decreases over the frequency. This is in contrast to hitherto known results but is confirmed by experiments conducted recently.

Acknowledgment

The authors wish to thank Dr. P. Saguet for his help and encouragement during the first part of this project.

References

[1] H. Hasegawa, M. Furukawa, and H. Yanai, "Properties of microstrip on Si–SiO_2 system," *IEEE Trans. Microwave Theory Tech.*, vol. MTT-19, pp. 869–881, 1971.

[2] D. Jager, W. Rabus, and W. Eichkoff, "Bias dependent small-signal parameters of Schottky contact microstrip lines," *Solid-State Electron*, vol. 17, pp. 777–783, 1974.

[3] Y. Fukuoka, Y. Shih, and T. Itoh, "Analysis of slow-wave coplanar waveguide for monolithic integrated circuits," *IEEE Trans. Microwave Theory Tech.*, vol. MTT-31, pp. 567–573, 1983.

[4] R. Sorrentino, G. Leuzzi, and A. Silbermann, "Characteristics of metal–insulator–semiconductor coplanar waveguides for monolithic microwave circuits," *IEEE Trans. Microwave Theory Tech.*, vol. MTT-19, pp. 869–881, 1971.

[5] A. A. Azeim, H. El Hennawy, and S. Mahrous, "Analysis of fin-lines on semiconductor substrate," in *Proc. 14th European Microwave Conf.* (Liege, Belgium), 1984, pp. 346–351.

[6] C. Seguinot, P. Kennis, P. Pribetich, and J. P. Villotte, "MIS slow-wave coplanar line: A comparison of theoretical and experimental characteristics," in *Proc. 16th European Microwave Conf.* (Dublin), 1986, pp. 445–446.

[7] T. C. Mu, H. Ogawa, and T. Itoh, "Characteristics of multiconductor asymmetric slow-wave microstrip transmission lines," *IEEE Trans. Microwave Theory Tech.*, vol. MTT-34, pp. 1471–1477, 1986.

[8] C. K. Tzuang and T. Itoh, "Finite-element analysis of slow-wave Schottky contact printed lines," *IEEE Trans. Microwave Theory Tech.*, vol. MTT-34, pp. 1483–1489, 1986.

[9] C. M. Krowne and E. J. Cukauskas, "GaAs slow-wave phase shifter characteristics at cryogenic temperature," *IEEE Trans. Electron Devices*, vol. ED-34, pp. 124–129, 1987.

[10] M. Aubourg *et al.*, "Analysis of M. I. S. or Schottky contact coplanar lines using the FEM and SDA," in *IEEE MTT-S Int. Microwave Symp. Dig.* (Boston), June 1983, pp. 396–398.

[11] K. Wu, "Structures hybrides planaires en vue de la realisation des dephaseurs variables integres," Ph.D. thesis (in French), Enserg-INPG, France, Oct. 1987.

[12] C. M. Krowne, "Slow-wave propagation in generalized cylindrical waveguides loaded with a semiconductor," *Int. J. Electron.*, vol. 58, no. 2, pp. 249–269, 1985.

[13] V. M. Hietala, Y. R. Kwon, and K. S. Champlin, "Loss-loss slow-wave propagation along a microstructure transmission line on a silicon surface," *Electron. Lett.*, vol. 22, pp. 755–756, 1986.

[14] Y. R. Kwon, V. M. Hietala, and K. S. Champlin, "Quasi-TEM analysis of 'slow-wave' mode propagation on coplanar microstructure MIS transmission lines," *IEEE Trans. Microwave Theory Tech.*, vol. MTT-35, pp. 545–551, 1987.

[15] K. Wu, "New prospective coplanar metal–insulator–semiconductor (MIS) monolithic structure," *Electron. Lett.*, vol. 24, pp. 262–264, 1988.

[16] K. Wu, A. Coumes, and P. Saguet, "New generalized computations of quasi-planar waveguides characteristics," *Int. J. Infrared and Millimeter Waves*, vol. 8, no. 3, pp. 241–282, 1987.

[17] U. Schulz and R. Pregla, "A new technique for the analysis of the dispersion characteristics of planar waveguides and its application to microstrip with tuning septums," *Radio Sci.*, vol. 16, no. 6, pp. 1173–1178, 1981.

[18] H. Diestel and S. B. Worm, "Analysis of hybrid field problems by the method of lines with nonequidistant discretization," *IEEE Trans. Microwave Theory Tech.*, vol. MTT-32, pp. 633–638, 1984.

[19] R. Pregla, M. Koch, and W. Pascher, "Analysis of hybrid waveguide structures consisting of microstrips and dielectric waveguides," in *Proc. 17th European Microwave Conf.* (Rome, Italy), 1987, pp. 927–932.

[20] K. Wu and R. Vahldieck, "Propagation characteristics of MIS transmission line with inhomogeneous doping profile," *IEEE Trans. Microwave Theory Tech.*, vol. 38, pp. 1872–1878, Dec. 1990.

[21] E. Yamashita and K. Atsuki, "Analysis of microstrip-like transmission lines by nonuniform discretization of integral equations," *IEEE Trans. Microwave Theory Tech.*, vol. MTT-24, pp. 195–200, 1976.

[22] W. Heinrich, "Full-wave analysis of conductor losses on MMIC transmission lines," in *IEEE MTT-S Int. Microwave Symp. Dig.* (Long Beach), June 1989, pp. 911–914.

[23] G. L. Matthaei, K. Kiziloglu, N. Dagli, and S. I. Long, "The nature of the charges, currents, and fields in and about conductors having cross-sectional dimensions of the order of a skin depth," *IEEE Trans. Microwave Theory Tech.*, vol. 38, pp. 1031–1036, 1990.

[24] K. Wu and R. Vahldieck, "A self-consistent approach to determine loss properties in MIC/MMIC coplanar transmission lines," in *Proc. 3rd Asia–Pacific Microwave Conf. (APMC'90)* (Tokyo, Japan), Sept. 1990, paper 35-4.

[25] Y-C. Shih and M. Maher, "Characterization of conductor-backed coplanar waveguide using accurate on-wafer measurement techniques," in *IEEE MTT-S Int. Microwave Symp. Dig.* (Dallas), May 1990, pp. 1129–1132.

[26] T. Shibata and E. Sano, "Characterization of MIS structure coplanar transmission lines for investigation of signal propagation in integrated circuits," *IEEE Trans. Microwave Theory Tech.*, vol. 38, pp. 881–890, 1990.

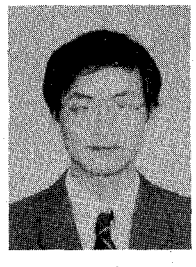

Ke Wu (M'87) was born in Jiangsu, China, on December 9, 1962. He received the B.Sc. degree (with distinction) in radio engineering from the Nanjing Institute of Technology (Now Southeast University), Nanjing, China, in 1982 and the D.E.A. degree in electronics and the Ph.D. degree (with distinction) in optics, optoelectronics, and microwave engineering from the Institut National Polytechnique de Grenoble (INPG), Grenoble, France, in 1984 and 1987, respectively.

During the years 1983–1987, he conducted research in the Laboratoire d'Eléctromagnetisme, Microondes et Optiques guidés (LEMO), Grenoble, France. Since 1988 he has been a postdoctoral research associate in the Department of Electrical and Computer Engineering at the University of Victoria, Victoria, B.C., Canada. His main research interests include electromagnetic fields, numerical methods, analysis and design of various microwave/millimeter-wave integrated and monolithic circuits, electro-optic and optoelectronic components, lightwave transmission systems, planar antennas and microwave/optical signal processing.

Dr. Wu received a Chinese Overseas Graduate Fellowship in 1982, a U.R.S.I. Young Scientist Award in 1987, and, together with two coau-

thors, the Oliver Lodge Premium from the IEE for the outstanding publication in 1988.

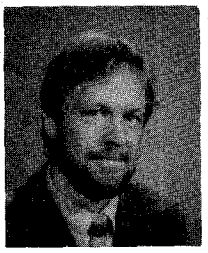

Rüdiger Vahldieck (M'85–SM'86) received the Dipl.-Ing. and Dr.-Ing. degrees in electrical engineering from the University of Bremen, West Germany, in 1980 and 1983, respectively.

From May 1984 to June 1986 he was a Research Associate at the University of Ottawa, Canada, and in July 1986 he joined the Department of Electrical and Computer Engineering at the University of Victoria, Victoria, B.C., Canada, where he is now an Associate Professor. His research interests include numerical methods to model electromagnetic fields for computer-aided design of microwave, millimeter-wave, and optoelectronic integrated circuits. He is also interested in design aspects of passive and active planar and quasi-planar components and filters for MMIC and MHMIC applications. Recently he has been involved in research on subcarrier multiplexed lightwave systems. The emphasis of this work is on broad-bandwidth electro-optic modulators and on coherent detection systems in fiber-optic communication links.

Dr. Vahldieck, together with three coauthors, received the outstanding publication award of the Institution of Electronic and Radio Engineers in 1983. He is on the editorial board of the IEEE TRANSACTIONS ON MICROWAVE THEORY AND TECHNIQUES and he has published more than 70 technical papers in the field of microwave CAD. He teaches professional short courses at the George Washington University, Washington, DC, on numerical techniques in electromagnetics.